Journal of Materials Processing Technology 222 (2015) 287–300

Contents lists available at ScienceDirect

Journal of Materials Processing Technology

journal homepage: www.elsevier.com/locate/jmatprotec

Effects of incremental depth and tool rotation on failure modes and microstructural properties in Single Point Incremental Forming of polymers

Mohammad Ali Davarpanah[a], Amin Mirkouei[b], Xiaoyan Yu[c], Rajiv Malhotra[a,*], Srikanth Pilla[c,d,**]

[a] Department of Mechanical Engineering, Oregon State University, United States
[b] Department of Industrial Engineering, Oregon State University, United States
[c] Department of Automotive Engineering, Clemson University, United States
[d] Department of Materials Science and Engineering, Clemson University, United States

ARTICLE INFO

Article history:
Received 26 November 2014
Received in revised form 2 February 2015
Accepted 7 March 2015
Available online 20 March 2015

Keywords:
Single Point Incremental Forming
Thermoplastics
Incremental depth
Tool rotation
Failure modes
Part microstructure

ABSTRACT

Single Point Incremental Forming (SPIF) is a sheet forming process characterized by advantages that include low-cost and part-shape-independent tooling, higher formability and greater process flexibility as compared to conventional sheet forming. While recent work has demonstrated the possibility of SPIF of polymers the effects of incremental depth and tool rotation speed, key process parameters in SPIF, have rarely been examined. This work experimentally examines how incremental depth and tool rotation speed affect the failure mode during forming, forming forces as well as the void structure and crystallinity of the formed material in polymer SPIF. The dependence of both tearing and wrinkling on the incremental depth and tool rotation speed is uncovered. It is shown that contrary to SPIF of metals, greater incremental depths result in increased formability in polymer SPIF, but this advantage is limited by the occurrence of sheet wrinkling at excessively high incremental depths. Further, the occurrence of sheet wrinkling depends not just on the incremental depth but also on the part shape being formed. Microstructural examination of the formed material shows that greater incremental depth results in greater void densities and that the material formed with SPIF has greater crystallinity than the unformed material. Additionally, it is shown that higher tool rotation speed can cause earlier onset of wrinkling. The implications of these observations on SPIF of polymers are discussed.

1. Introduction

Single Point Incremental Forming (SPIF) is a process in which a completely peripherally clamped sheet of material is locally deformed by a small hemispherical ended tool moving along a predefined toolpath. These local deformations accumulate to give the sheet its final desired shape. A significant amount of research has been performed on SPIF of metals in terms of deformation and fracture mechanics, forming forces, toolpath planning, geometric accuracy and surface finish in the process. Recent work on SPIF of polymers has also uncovered the possibility of expanding the materials capability window of SPIF beyond metals, by demonstrating SPIF of thermoplastic polymers at room temperature. This creates the possibility of saving on both tooling costs as well as on the thermal energy costs, which are inherent in injection molding or thermoforming processes that are typically used to fabricate freeform thermoplastic surfaces. Further, cold-state SPIF results in reduced heating of the sheet which is highly desirable for temperature sensitive biopolymers such as polylactic acid (PLA) and polyhydroxyalkanoates (PHAs). This lowered heating can alleviate thermal degradation and retain the virgin material properties that would have been lost in conventional fabrication processes. Past work on polymer SPIF has performed both experimental and computational investigations. Franzen et al. (2009) experimentally examined the feasibility of forming polyvinyl chloride (PVC) sheets into axi-symmetric shapes using SPIF. The following three modes of sheet failure were observed:

* Corresponding author at: Department of Mechanical Engineering, Oregon State University, United States. Tel.: +1 7734998942.
** Corresponding author at: Department of Automotive Engineering, Department of Materials Science and Engineering, Clemson University, United States Tel: (864) 283-7216.
E-mail addresses: malhotra@onid.oregonstate.edu (R. Malhotra), spilla@clemson.edu (S. Pilla).

http://dx.doi.org/10.1016/j.jmatprotec.2015.03.014
0924-0136/

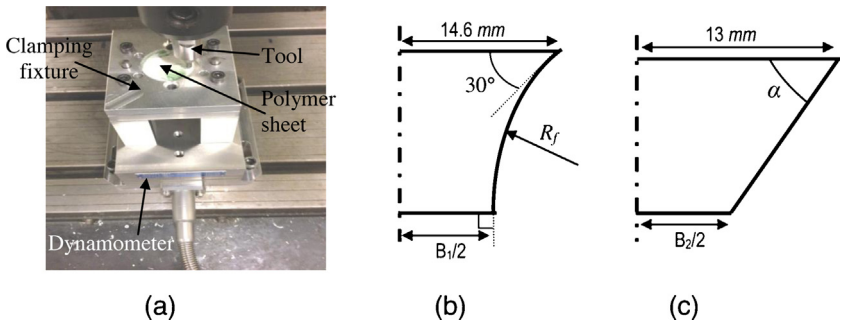

Fig. 1. (a) SPIF setup, (b) profile of formed funnel shape, and (c) profile of formed cone shape.

Mode 1: Sheet fracture by ductile tearing along the circumferential direction, at the transition between the wall and the corner radius of formed parts.
Mode 2: Wrinkling of the sheet along the wall of the part.
Mode 3: Tearing of the sheet in the radial direction, along the wall of the part.

The authors noted that only Mode 1 failure is typically seen in SPIF of metals and that Mode 3 failure is probably due to the occurrence of defects in the as-received sheet. The authors also showed stress whitening in the formed PVC material, and noted that this was probably due to deformation induced crazing in PVC. Martins et al. (2009) further extended the above work to show that a reduction in tool radius and an increase in the sheet thickness result in increased formability in polymer SPIF, much like in metals SPIF. Franzen et al. (2008) performed SPIF of five different polymers with varying degrees of crystallinity. It was shown that the reduction in density of the formed PVC material was larger than that of materials like polycarbonate and polyamide. The authors also experimentally demonstrated that the change in formed material density depends on the wall angle of the part being formed, and therefore on the strain induced in the material during SPIF. Furthermore, the dependence of springback on the sheet material properties was qualitatively examined in terms of the ratio of the yield stress of the material to the product between the thickness and elasticity modulus of the sheet material. Silva et al. (2010) focused on computationally examining the deformation mechanics in polymer SPIF by extending the membrane-based analysis developed by Martins et al. (2008) via a pressure modified Tresca yield criterion. This single-step analysis models only Mode 1 failure by tearing and considers the influence of part shape, tool diameter, sheet thickness and mechanical properties of the polymer sheet on tearing in polymer SPIF. The authors successfully predicted experimental observations that reducing the tool radius can increase the formability of the material, more so for thicker sheets than for thinner sheets. However, due to the single-step nature of analysis this technique did not account for the effects of incremental depth (Δz) on Mode 1 and Mode 2 failure. The above literature review shows that the effects of incremental depth Δz and tool rotation ω on polymer SPIF have rarely been explored till date. The basis for expecting an effect of Δz, especially on the sheet failure modes, arises from the fundamental nature of deformation in SPIF in which a change in Δz can create a change in the stress history imposed on the sheet material. Past work on metal SPIF Xu et al. (2013) has shown that tool rotation, and the resulting frictionally generated heat, can significantly increase formability and reduce the forming forces. A similar effect can be expected in polymer SPIF as thermoplastics exhibit softening and increase in ductility when heated.

This paper characterizes the effects of Δz and ω on failure, forming forces, as well as void content and crystallinity of the formed material in polymer SPIF. The experiments performed are described in Section 2. Section 3 describes the observed effects of Δz and ω on failure modes. We go beyond just Mode 1 failure and uncover a distinct transition between Mode 1 and Mode 2 failure that is dependent on the above process parameters as well as on the part shape being formed. Furthermore, the effects of Δz and ω on void density and crystallinity of the formed material are obtained via Scanning Electron Microscopy and Differential Scanning Calorimetry. Section 4 discusses the implications of these observations in terms of failure modes during polymer SPIF, process throughput and formed material properties, along with a discussion on possible directions for future work.

2. Experimentation

An SPIF setup with a circular forming area of 40 mm diameter was assembled on a HAAS CNC machine platform (Fig. 1a). This setup consisted of the following components: (i) the clamped polymer sheet, (ii) the blankholder mounted onto a Kistler 9257B plate type dynamometer, and (iii) the forming tool mounted on the CNC spindle. The dynamometer was mounted onto the bed of the CNC and was used to monitor the forming forces during SPIF. No backing die was used and a PTFE-based grease was used as the lubricant at the tool sheet interface during all experiments.

To examine the effect of Δz and ω on failure modes two kinds of part shapes were formed namely, funnel shapes (Fig. 1b) with continuously varying wall angle from 30° to 90° and a variable radius of curvature R_f and cone shapes (Fig. 1c) with variable wall angle α. For the funnel shape the base diameter B_1 varied from a minimum of 8.1–16 mm whereas for the cone shape the base diameter varied from 8.6–17 mm. Since a tool of diameter 5 mm was used in all the SPIF experiments shown in this paper there was no interference of the tool with the already formed region of the sheet during forming.

The funnel shape has been frequently used to examine formability in metal SPIF (Hussain and Gao, 2007) since its geometry provides a continuously increasing strain to be imposed on the sheet during deformation. On the other hand the constant wall angle of the cone shape results in a more uniform strain being imposed along the wall of the formed part. SPIF experiments were

Table 1
Summary of experimental parameters used.

Material	Incremental depth Δz (mm)	Tool rotation speed ω (rpm)	R_f (mm)	α (degrees)
PLA	0.2, 0.4, 0.6, 0.8, 1.0	0, 1250, 5000, 7000	10, 12, 14, 16	55, 65, 75
PVC	0.2, 0.6, 1.0, 1.4, 1.8	0, 1250, 5000, 7000		

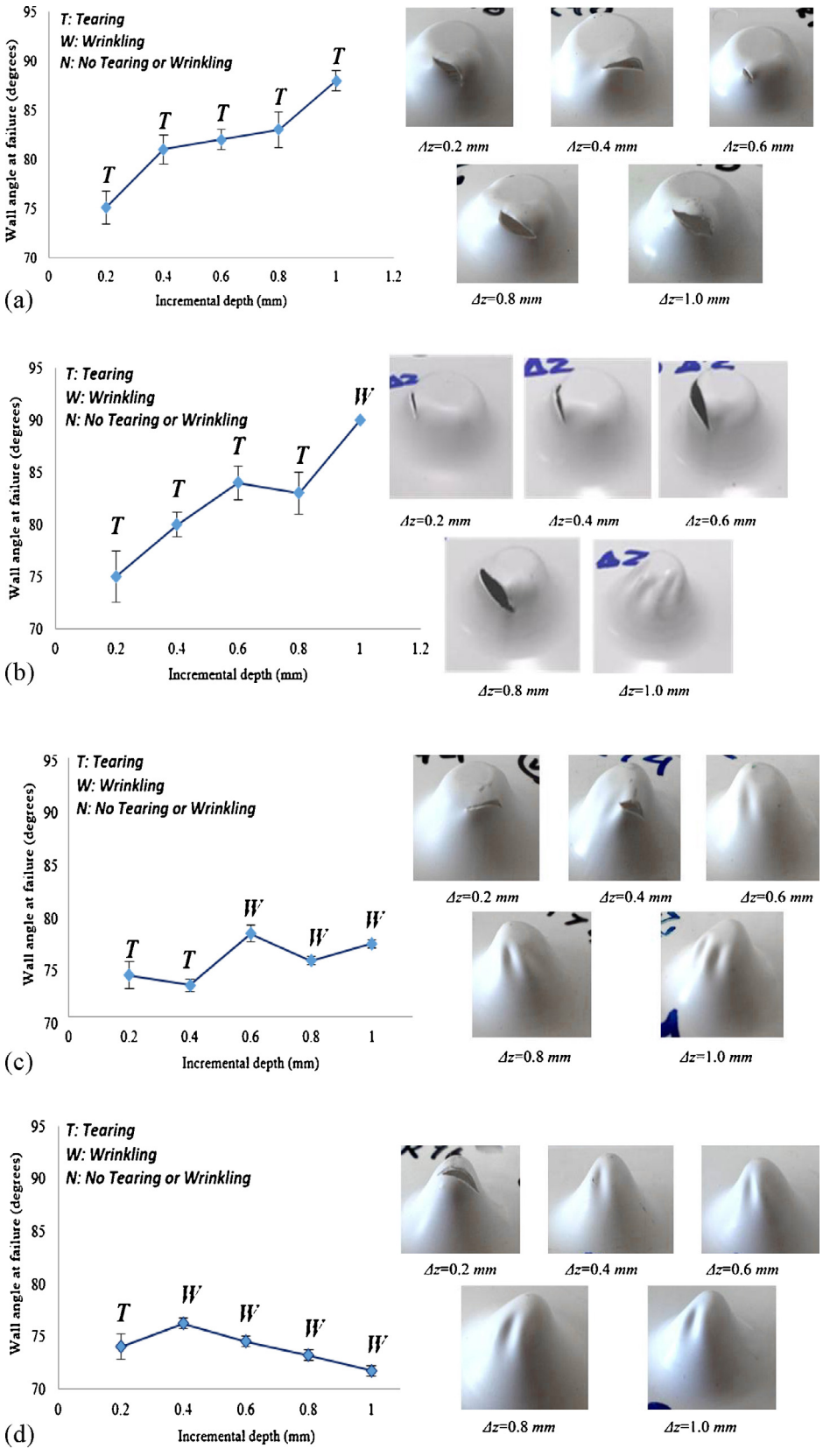

Fig. 2. Effect of Δz on failure modes and formed parts for funnel shaped PLA parts with R_f = (a) 10 mm, (b) 12 mm, (c) 14 mm, and (d) 16 mm.

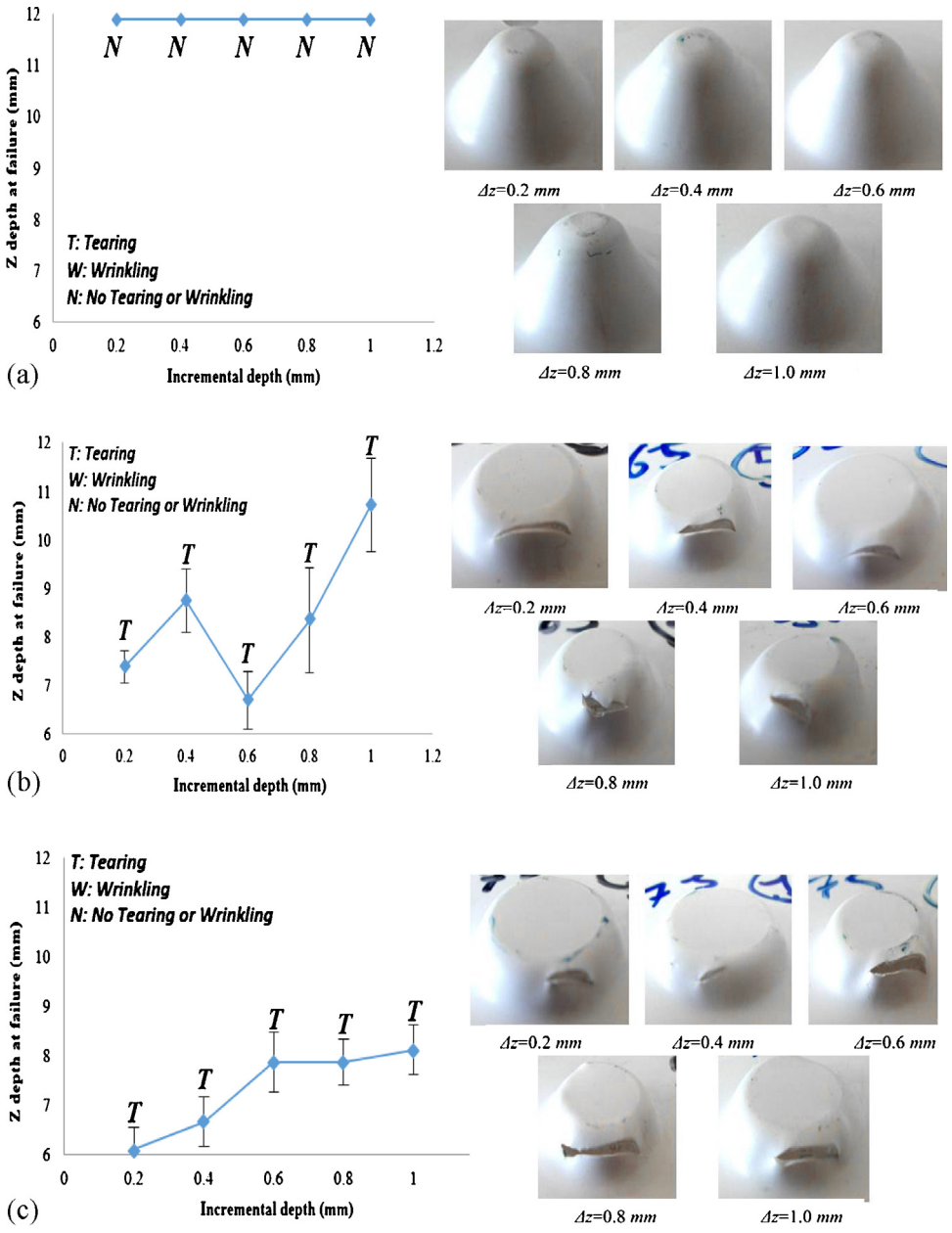

Fig. 3. Effect of Δz on failure modes and formed parts for PLA cone parts with α = (a) 55°, (b) 65°, and (c) 75°.

performed with contour toolpaths generated from the CAD geometry of the part using automated toolpath generation methods after Malhotra et al. (2010). Two polymer sheets, i.e., a 1.5 mm thick petroleum-based PVC material and 0.7 mm thick bio-based polylactic acid (PLA) material, were used as blank materials. The blank material was confined to these polymers because our goal was not to compare the ability of SPIF to form different thermoplastic materials but to examine the effects of Δz and ω on polymer SPIF in general.

A range of incremental depths from 0.2 mm upto a value greater than the sheet thickness were used to generate the toolpaths. The tool feed rate and tool diameter were kept constant at 300 mm/min and 5 mm respectively. The sheet thickness, tool feed rate and tool diameter were kept constant since the effect of these parameters has been shown in past literature. Table 1 summarizes the values of experimental parameters Δz and ω as well as the values of the shape parameters R_f and α used in the experiments. Only Mode 1 and Mode 2 failure were seen in this work and so only these failure modes are reported. The tool tip depth at failure during SPIF was recorded during forming experiments and was converted into the corresponding wall angle by using the CAD model of the desired part, the forming tool diameter and the designed toolpath. Each experiment was performed at least four times.

3. Experimental observations and discussion

This section discusses the results of the above experiments in terms of the sheet failure modes, forming forces as well as the measured void structure and crystallinity of the formed material.

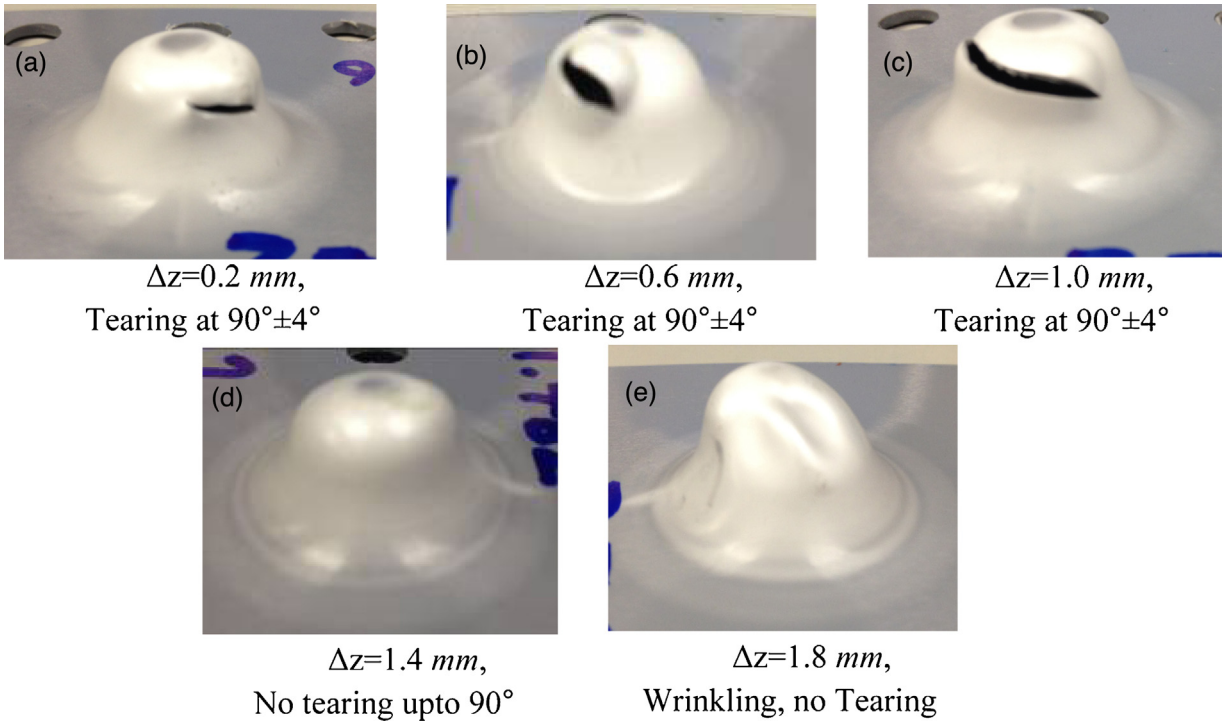

Fig. 4. Formed parts showing the effect of Δz on sheet tearing or wrinkling for SPIF of PVC funnel part with R_f = 12 mm.

3.1. Failure modes

Fig. 2 shows the effect of Δz, at ω = 0 rpm, on the maximum formable wall angle in SPIF of the PLA funnel shapes. In these plots the data points are supplemented with a description of whether tearing (i.e., Mode 1 failure, denoted as T), wrinkling (i.e., Mode 2 failure, denoted as W) or no failure (denoted as N) was observed. This kind of description is used throughout this paper. Fig. 2a shows that for R_f = 10 *mm*, as Δz increases there is an increase in the maximum formable wall angle and therefore in the formability. Furthermore, failure occurs by tearing and not by wrinkling.

At the same time, Fig. 2b shows that for R_f = 12 mm at Δz = 1.0 mm wrinkling appears as the mode of failure. Furthermore, as the value of R_f increases there is a reduction in the Δz value at which this transition between Mode 1 failure by tearing and Mode 2 failure by wrinkling occurs. A possible conclusion to draw from these observations, is that in polymer SPIF the formability increases with the Δz, but if the Δz is too high then unwanted sheet wrinkling might occur. Therefore, there is a transitional Δz at which the mode of failure transitions from Mode 1 failure by tearing to Mode 2 failure by wrinkling.

However, one must first consider past work in metals SPIF as well before accepting wrinkling as a universal phenomena in polymer SPIF. In past work on metals SPIF Jackson and Allwood (2009) have shown that SPIF is characterized by much larger shear stresses than are typically present in conventional forming. Computational analysis by Malhotra et al. (2012) showed that this shear plays a key role in formability in metals SPIF and that the magnitude of this shear depends on the shape of the part being formed. Hussain and Gao (2007) further observed that the formability in metals SPIF depends significantly on the part shape being formed. They formed funnel shapes with different radii of curvature of the wall to show that the formability changes with the radius of curvature. Since different part shapes (e.g., varying R_f for the funnel shape) result in different stress states and stress histories being imposed on the sheet the conclusion was that the formability and deformation mechanics in SPIF depend significantly on the stress state and stress history imposed on the material. In light of these observations it is useful to examine the effect of Δz on tearing and wrinkling for a part shape that is different than the funnel shape.

Fig. 3 shows the effect of Δz at ω = 0 *rpm* on the failure modes in SPIF of PLA cone shapes. Note that wrinkling does not occur at any Δz for the cone shape, irrespective of the wall angle. At the same time there is an increase in the formability with increasing Δz, shown by the increase in the formable depth at a constant wall angle. The lack of wrinkling in the cone shapes and its presence in the funnel shapes indicates that the occurrence of wrinkling also depends on the overall part shape being formed. Therefore, the constraint placed on maximum Δz usable due to the occurrence of wrinkling depends significantly on the part shape being formed. In fact, Fig. 2 shows a similar phenomena since a change in R_f causes a change in the mode of failure from tearing to wrinkling at the same incremental depth. For example at Δz = 1.0 mm tearing is observed in the case of R_f = 10 mm (Fig. 2a) whereas wrinkling is

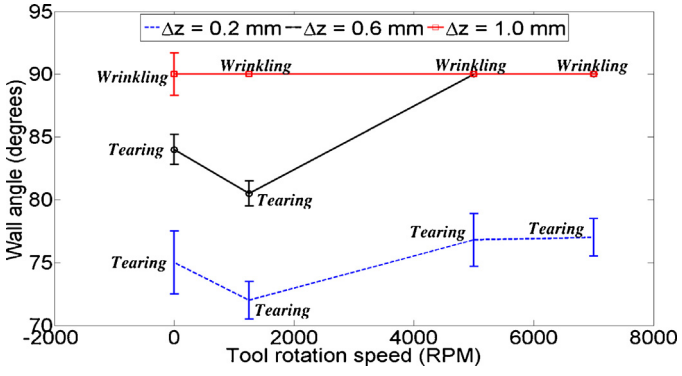

Fig. 5. Change in wall angle at tearing/wrinkling with Δz and ω for PLA funnel part.

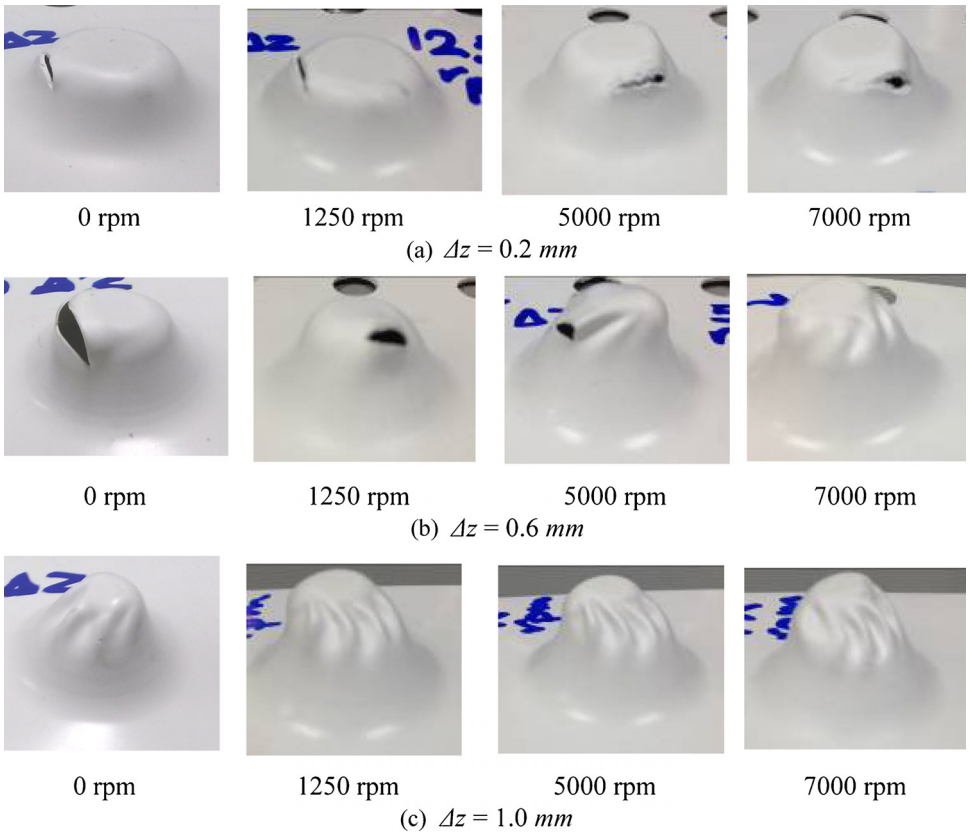

Fig. 6. Formed PLA funnel parts showing change in failure mode with change in Δz and ω.

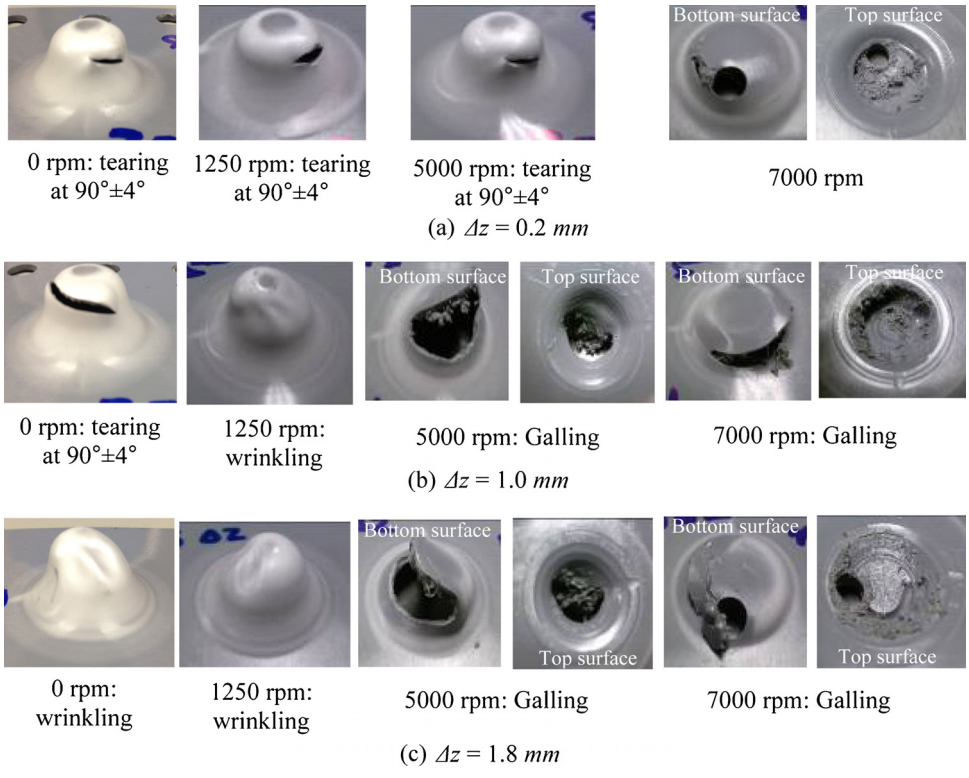

Fig. 7. Formed PVC funnel parts showing change in failure mode with change in Δz and ω.

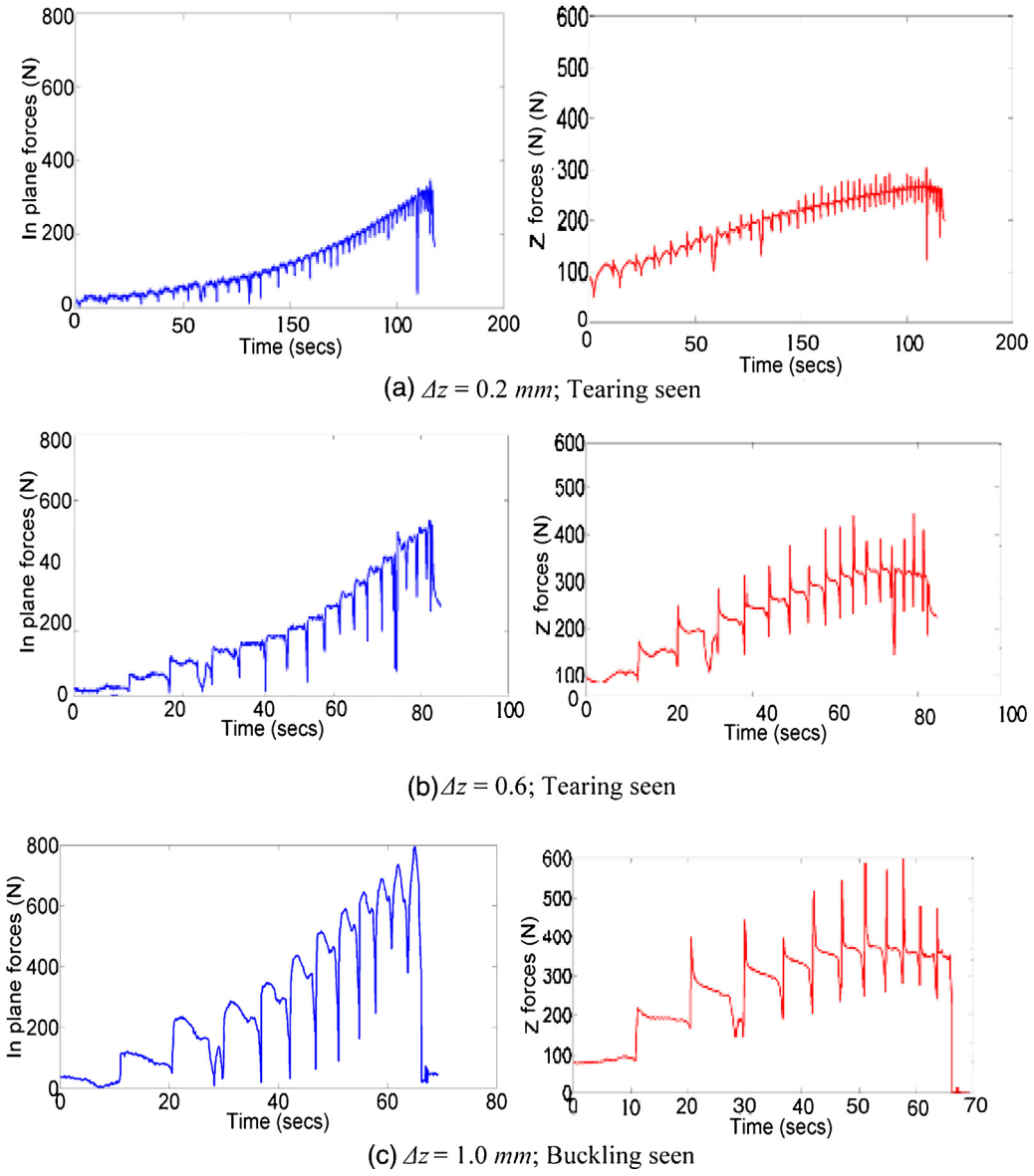

Fig. 8. In-plane and Z forming forces for PLA funnel part with R_f = 12 mm.

observed for R_f = 12 mm and above (Fig. 2b–d). These phenomena were also observed for PVC. An example of the transitional Δz for PVC is shown in Fig. 4 for the funnel shape with R_f = 12 mm.

Figs. 5 and 6 show the effect of increasing the tool rotation speed ω on the failure modes for the PLA funnel shape with R_f = 12 mm. It can be seen that increasing the tool rotation speed has very little positive effect on increasing the formability with Mode 1 failure (e.g., for Δz = 0.2 mm at 1250, 5000 and 7000 rpm in Fig. 6a, and for Δz = 0.6 mm at 1250 rpm in Fig. 6b). On the other hand, at a constant Δz an increase in ω increases the tendency for sheet wrinkling to occur (e.g., Δz = 0.6 mm at 5000 and 7000 rpm in Fig. 6c). For larger incremental depths (Δz = 1.0 mm) the increase in ω is unable to alleviate the occurrence of Mode 2 failure. Similar effects where observed when forming the funnel part with R_f = 12 mm on PVC sheets (Fig. 7).

Further, during SPIF of the PVC funnel shape it was observed that sheet galling occurred at tool rotation speeds of 5000 rpm and above, resulting in premature sheet failure. Similar effects of ω were observed for PLA and PVC for funnel shapes with different R_f values and for the cone parts as well. To summarize, tool rotation in polymer SPIF has minimal effect on the Mode 1 failure and greater tool rotation speed can increase the tendency of the sheet to undergo Mode 2 failure or galling during FPI.

3.2. Forming forces

Past work (Filice et al., 2006; Duflou et al., 2007; Bouffioux et al., 2008) in metals SPIF has shown that the forming forces in SPIF indicate key characteristics of the process mechanics. Further forming forces are a critical process metric needed for process model calibration and machine design. Figs. 8 and 9 show representative in-plane and Z forces as a function of Δz when ω = 0 for R_f = 12 mm funnels. The in-plane forces were obtained as the magnitude of the resultant of the X and Y forces. As typically seen in a contour toolpath (Duflou et al., 2007), after the completion of one contour the Z force drops when the tool moves to the next contour, reaches its

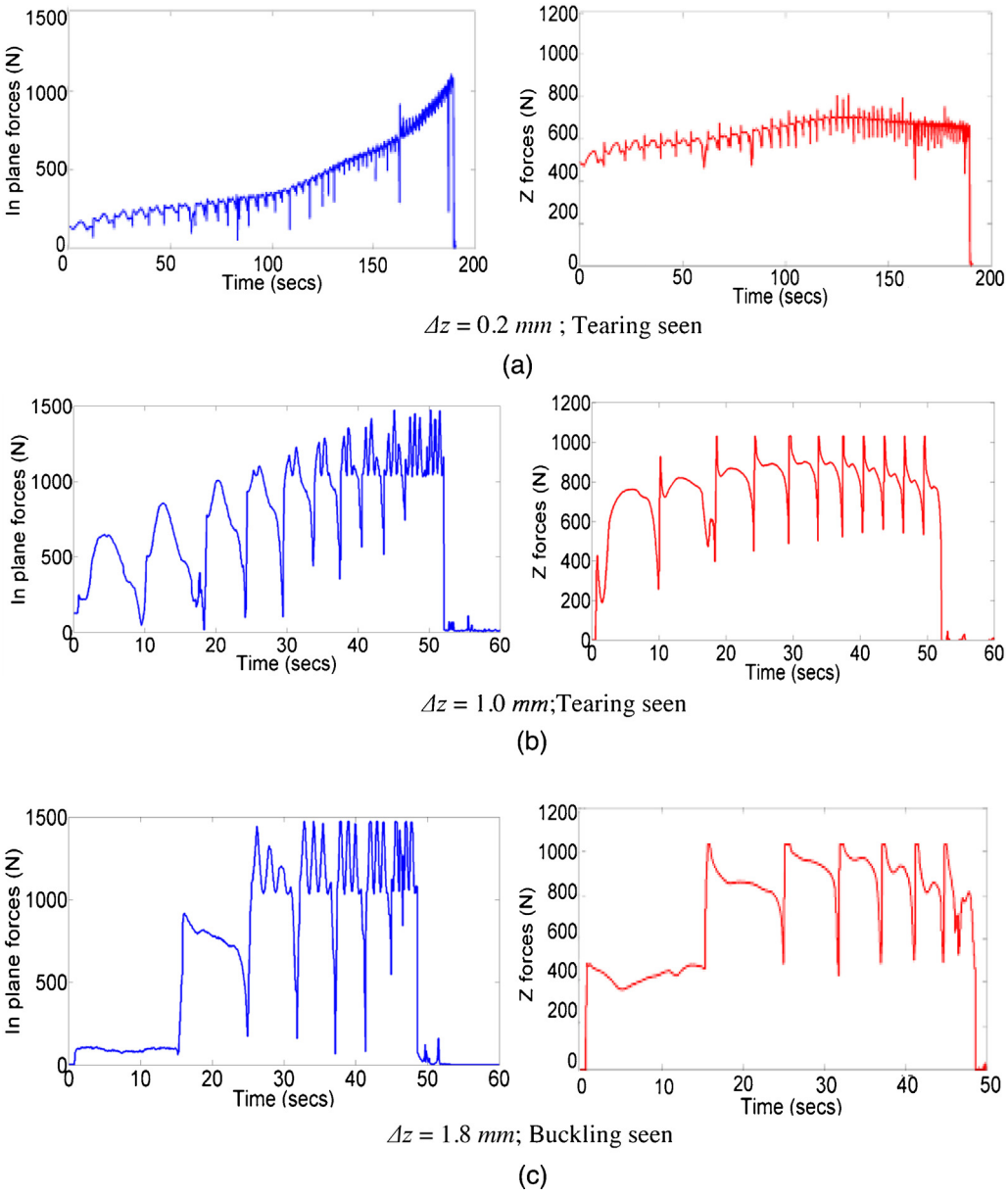

Fig. 9. In-plane and Z forming forces for PVC funnel part with R_f = 12 mm.

peak value at the step down and finally stabilizes when the tool moves along the contour.

The stable portions of the in-plane and Z forces were obtained for the above performed experiments after filtering out the spikes at the step down of the contour path. The filtering was done via a nonlinear median filtering algorithm which applies a sliding window to a sequence of data and replaces the center value in the window with the median value of all the points within the window (Pratt, 1991). Fig. 10 compares the peak in-plane and Z forces over a range of Δz and ω for R_f = 12 mm funnels formed on both PLA and PVC. Fig. 10 shows that there is an increase in the in-plane and the Z forces with an increase in Δz. This is a typical trend that is also seen in SPIF of metals and is related to a larger amount of material being deformed in each contour as the Δz increases. Further, there is a steady reduction in the in-plane and Z forces with an increase in tool rotation speed. This is probably due to frictional heat generated at the tool-sheet interface. Further, this implies that if formability constraints can be met and the occurrence of buckling or galling can be prevented, then increasing tool rotation speed can enable forming of thicker sheets with lower forming forces.

Note that the increase in the in-plane forming forces with an increase in Δz is more significant than that for the Z forces, and is simultaneously accompanied by a transition from tearing to wrinkling (Figs. 6 and 7). It might be hypothesized that these increased X and Y forces are responsible for sheet wrinkling due to dragging the sheet along with the tool. However, there is also a reduction in in-plane forces with an increase in tool rotation speed but no alleviation of wrinkling which shows that the above hypothesis may not always be true.

3.3. Void structure in formed material

Figs. 11 and 12 show representative scanning electron microscope images of the formed and as received material for the funnel

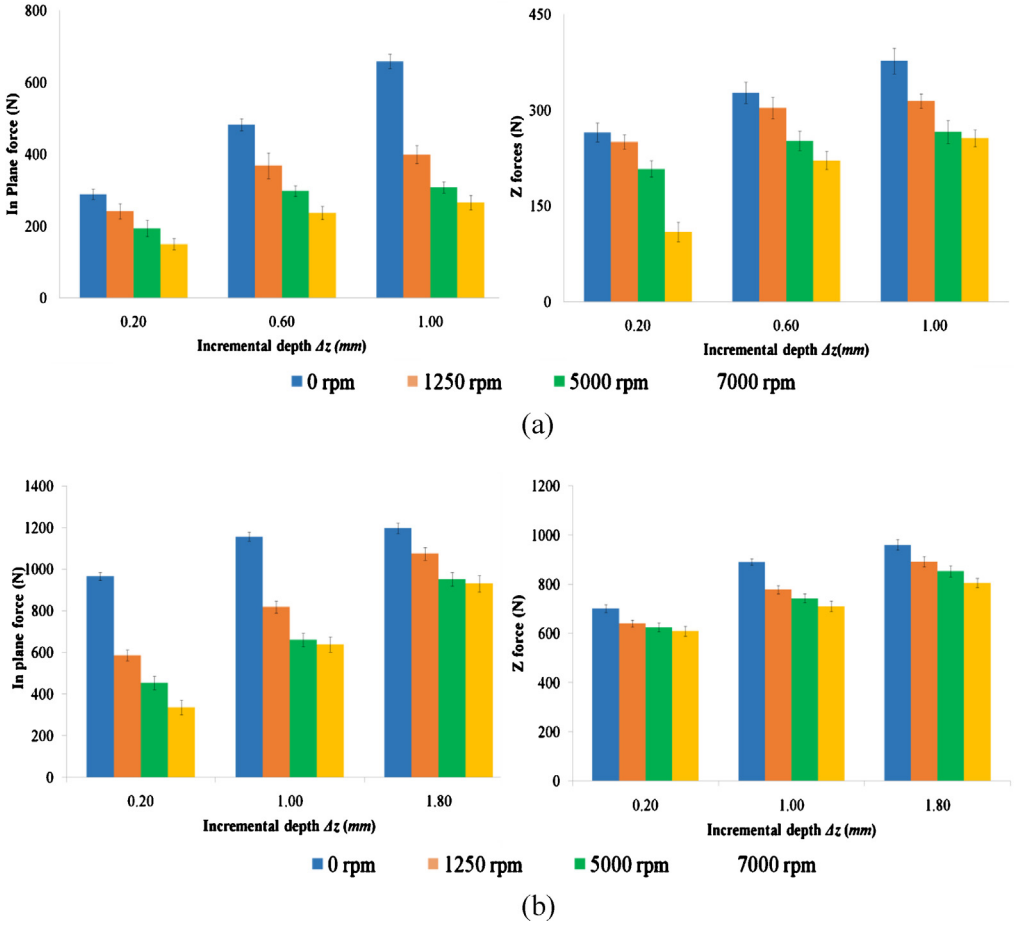

Fig. 10. Comparison of maximum stable in-plane and Z forces at different incremental depths and tool rotation speeds for funnel part with R_f = 12 mm formed on (a) PLA and (b) PVC.

parts with R_f = 12 mm, on PLA and PVC respectively. The outer surface of the formed material (the side of the sheet that was not in contact with the tool during SPIF) was examined as this is the region of the material where material fracture initiates (Malhotra et al., 2012). The samples were taken from the middle of the formed wall of the funnel parts. Note that for PVC we ignore the cases where sheet galling occurred (Δz = 0.2 mm at 7000 rpm; Δz = 1.0 mm at ω = 5000, 7000 rpm; Δz = 1.8 mm at ω = 5000, 7000 rpm). This is because galling resulted in premature failure so that insignificant changes in void structure were observed because of an insignificant amount of deformation.

Fig. 13a and b shows the void density and average void area obtained by averaging over a larger number of SEM images. Given that the average cell area is fairly constant for different Δz and tool rotation speeds the trends for the void area fraction, i.e., the surface area of voids to the total surface area, is expected to follow the trends for the void density. For Δz = 0.2 mm the void density at ω = 1250 rpm is lower than that at ω = 0 rpm. There is again a slight increase when the ω = 7000 rpm. This reflects the trend for dependence of formable wall angle on tool rotation speed at Δz = 0.2 mm (Fig. 5) where the maximum formable wall angle by tearing sees a slight dip at 1250 rpm and then an increase at 7000 rpm. The dependence of void density on tool rotation speed is similar for Δz = 1.0 mm (Fig. 10a). However, an anomaly is noticed for the Δz = 0.6 mm case at 7000 rpm where the void density is lowest as compared to that at the other tool rotation speeds Δz = 0.6 mm.

A key point to note is that despite the above anomaly the void density, and thus the void area fraction, is consistently higher at greater Δz. This is despite the fact that at higher Δz the wall angle at tearing and therefore the formability is higher (Fig. 5). In the case of PVC (Fig. 13c and d) for Δz = 0.2 and 1.8 mm an increase in the tool rotation speed to 1250 rpm results in increased void density. An anomalous trend is seen for Δz = 0.6 mm where the void density reduces with an increase in the tool rotation speed. Since failure in PVC occurs at similar wall angles irrespective of the value of Δz or ω it is difficult to correlate void density to formability.

3.4. Thermal properties and crystallinity

The crystallization behavior of the formed and as-received PLA and PVC materials was studied using differential scanning calorimetry (TA Instruments, Q2000) via heat/cool/heat cycles. The samples were heated from 40 °C to 180 °C and kept isothermal for 3 minutes before cooling to 0 °C and then reheating up to 200 °C. The temperature ramp rate in all the cycles was 10 °C/min. The thermograms for PLA obtained from the first and second heating cycles are shown in Fig. 14a and b respectively. The data obtained from the first heating cycle provides information on the crystallinity of the PLA material formed by SPIF, whereas the data obtained from the second heating cycle allows for a direct comparison of the crystallization behavior after erasing any previous thermal history (caused

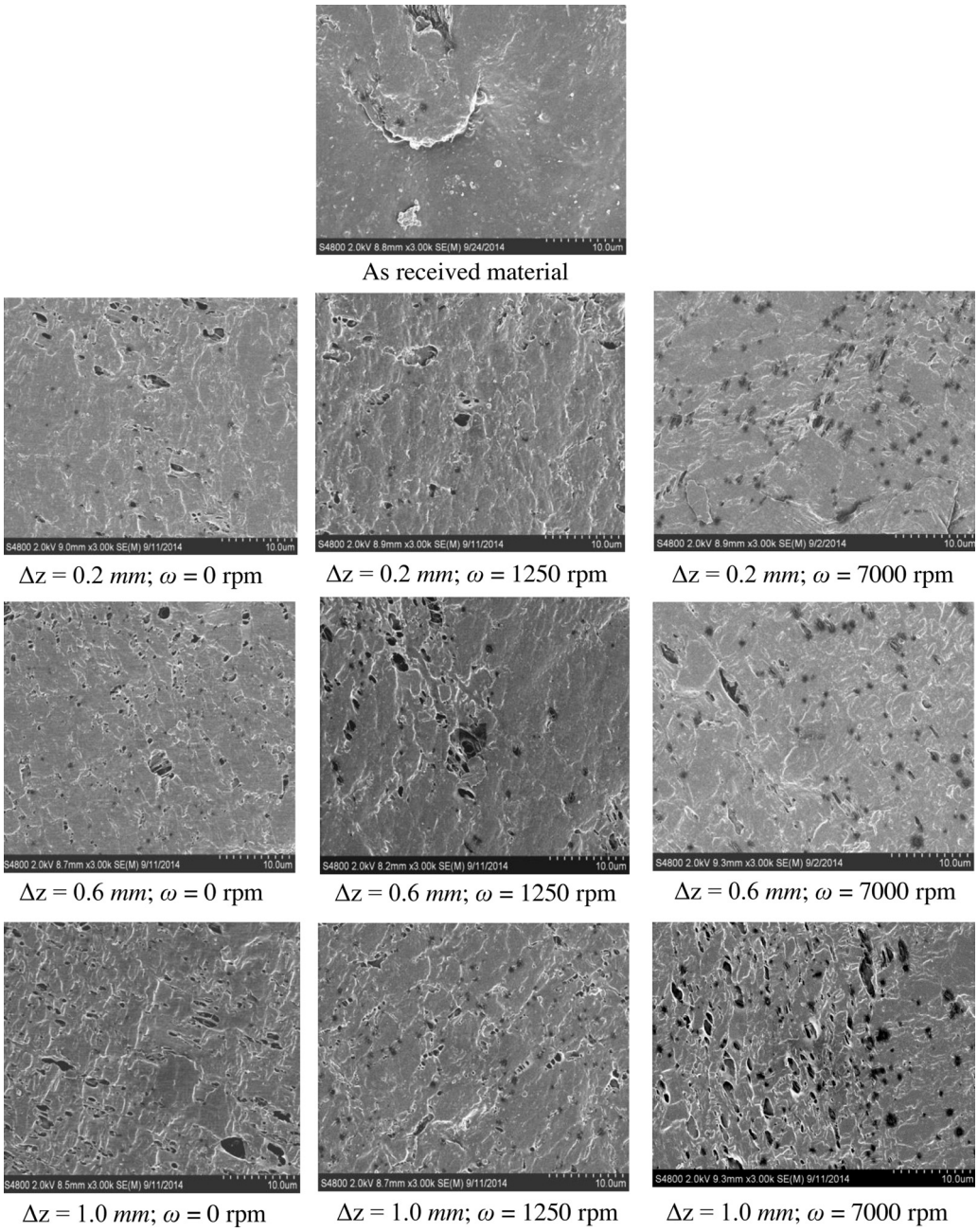

Fig. 11. SEM micrographs of PLA funnel part at different Δz and ω.

by SPIF) through the first heating cycle. The crystallinity of PLA is computed using the following equation (Pilla et al., 2008).

$$\chi_c = \frac{\Delta H_m - \Delta H_{CC}}{H_m^0} \cdot \frac{100}{w} \quad (1)$$

where χ_c = percentage of crystallinity, $\Delta H_m^0 = 93.7\,\mathrm{J/g}$, w = weight fraction of PLA in sample, ΔH_{cc} = cold-crystallization enthalpy. For the present study, the weight fraction of PLA was taken to be same for all the samples i.e., 100.

The PLA thermograms obtained from the first heating cycle show an endothermic peak (in all the specimens) near the glass transition (T_g) phase because of physical aging of the polymeric materials (Hodge, 1983a,b; Hodge and Berens, 1982). This phenomenon is related to the inherent distribution of the relaxation times of polymer chains (Turi, 1997). On the other hand, during the second heating cycle, the endotherm peaks near T_g were not observed. This is because the enthalpic recovery that occurred during the first heating cycle is kinetic in nature (Pilla et al., 2009). Fig. 14c shows that the SPIF process has enhanced the degree of crystallinity of as received PLA from 5.7% to ~10.5%.

Moreover, the increase in ω (0–7000 rpm) results in an even greater enhancement of the degree of crystallinity. A similar trend was observed for the degree of crystallinity computed from second heating cycle (Fig. 14d). However, the observed crystallinity is much higher than the first cycle. As mentioned, the first heating crystallinity reflects the crystal morphology induced by SPIF process while the second heating crystallinity

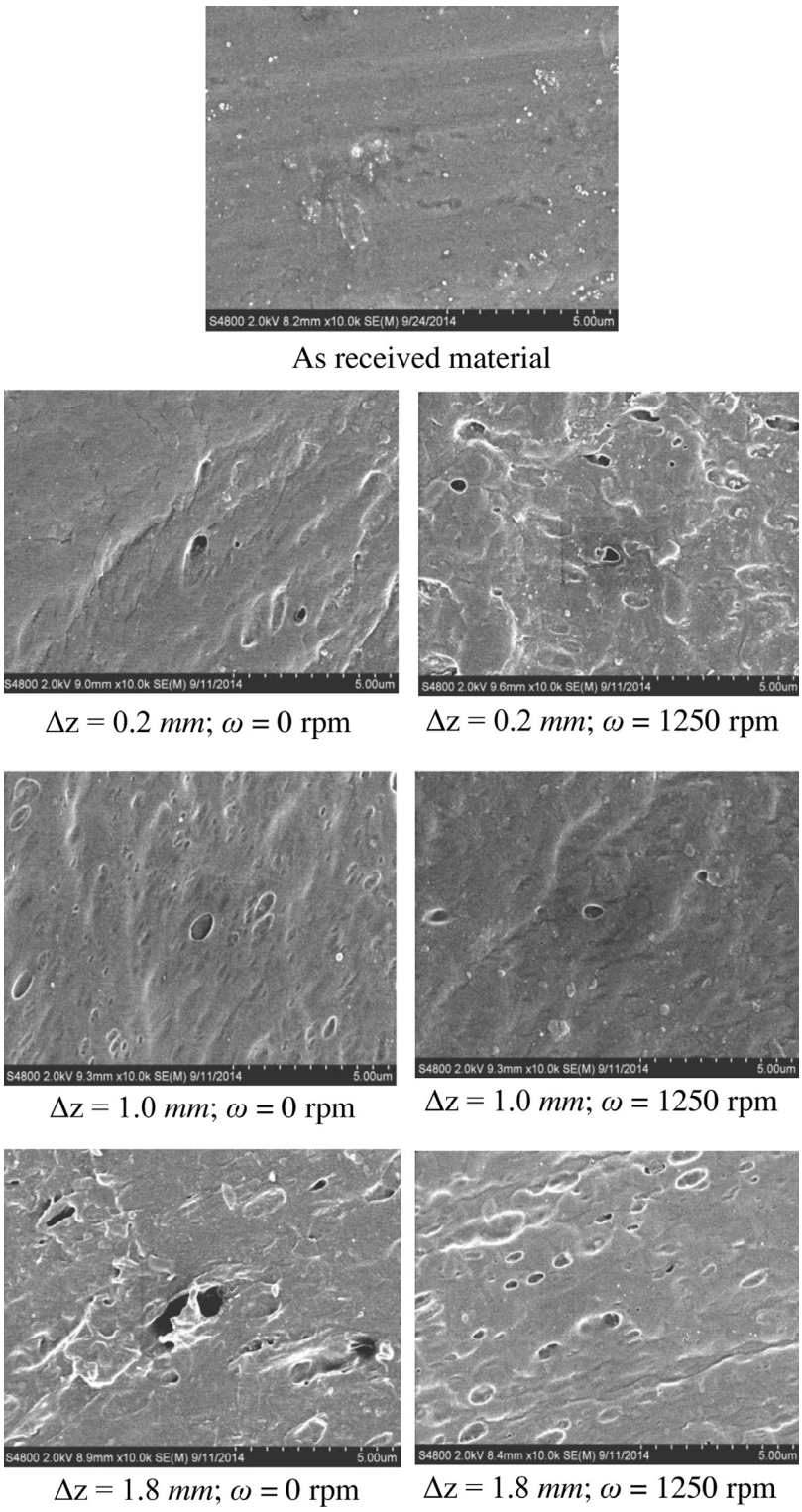

Fig. 12. SEM micrographs of PVC funnel part at different Δz and ω.

is induced due to cooling rate of cooling cycle. As discussed in the next section, the enhancement in crystallinity of PLA due to the SPIF process has significant implications especially on the mechanical properties of the formed material. The PVC material investigated in this study was completely amorphous (Fig. 15) and hence, unlike PLA, no crystal morphology was observed.

4. Discussions and future work

This section discusses the implications of the above experimental observations on polymer SPIF. Figs. 2 and 4 show that unlike SPIF of metals, in polymer SPIF there is an increase in the formability with increase in the incremental depth. This implies a dual advantage of increasing both the formability and the

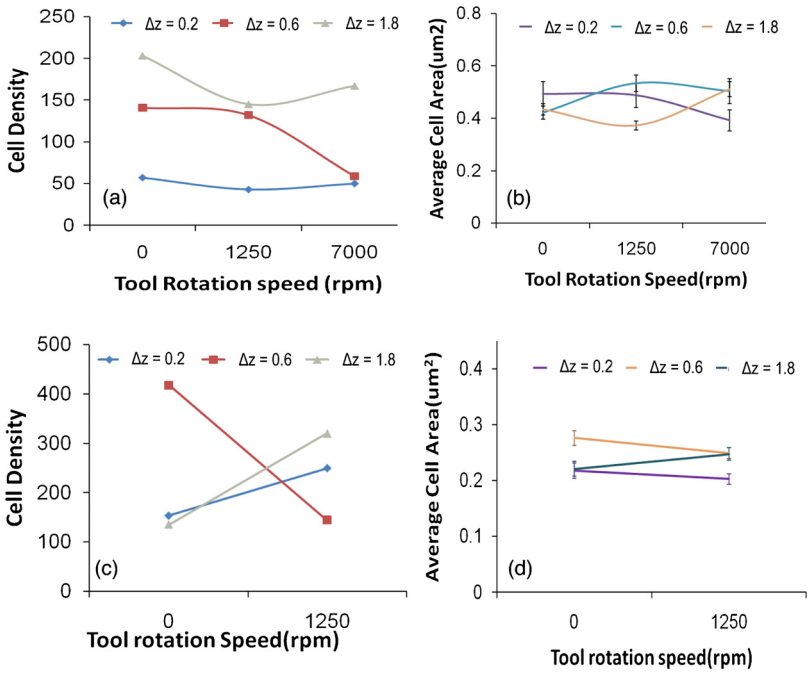

Fig. 13. (a) Void density for PLA, (b) average void area for PLA, (c) void density for PVC, and (d) average void area for PVC.

process throughput at the same time. However, Figs. 2 and 4 also show that there is a limit on this increase in incremental depth in the form of a transitional incremental depth beyond which the failure mode transitions from Mode 1 tearing failure to Mode 2 wrinkling failure. At the same time, Fig. 2 shows that this transitional incremental depth depends on the radius of curvature R_f of the part and Fig. 3 shows that the Mode 2 failure is absent in the forming of a cone shape. This implies that this transitional incremental depth depends on the part shape being formed. In summary, increasing the incremental depth increases the formability of the material in polymer SPIF while being limited by the occurrence of sheet wrinkling at high incremental depths, and the occurrence of this wrinkling additionally depends on the overall part shape as well. Therefore, there is an optimum value of the incremental depth, i.e., the transitional incremental depth at which formability and throughput can be simultaneously maximized. An investigation of the deformation mechanics that causes this phenomena and mechanics based prediction of this transitional incremental depth for any given part shape is needed.

Figs. 5–7 show that an increase in tool rotation speed does not significantly increase the formability of the material in polymer SPIF. On the other hand increasing the tool rotation speed causes an increased tendency for wrinkling. Further, in the case of PVC too high a tool rotation speed can also cause galling and premature failure of the sheet during forming.

Figs. 8–10 show that the forming forces rise with an increase in the incremental depth which is also observed in metals SPIF. Furthermore, with an increase in the tool rotation speed a reduction in the forming forces is observed (Fig. 10) which is probably due to greater friction at the tool-sheet interface. The simultaneous transition to wrinkling and the relatively larger increase in the in-plane forces at higher incremental depths might indicate that wrinkling is due to higher in-plane forces. However the alleviated occurrence of wrinkling despite a reduction in the in-plane forces with higher tool rotation speed does not agree with this hypothesis. At the same time if wrinkling or galling can be prevented then tool rotation might be usable for keeping process forces within machine limitations, especially when forming a thicker polymer or a polymer with higher yield stresses.

In Fig. 12 the relationship between void density and formability is not clear for PVC since the PVC funnels with $R_f = 12$ mm are almost always formed to nearly the same wall angle whether failure occurs or not (Fig. 4). However, the results shown for PLA in Figs. 2b and 11 show that an observably increased formability by tearing is accompanied by a corresponding increase of the void density in the formed material. The underlying deformation mechanics that cause this paradoxical effect need to be investigated further. Additionally, these observations suggests that due to greater void content a material formed with higher incremental depth may undergo earlier failure under mechanical loading conditions during part operation.

The enhanced crystallinity of the formed material as compared to the base material (Fig. 14c and d) might be due to strain-induced crystallization (SIC) that is observed in solid polymers (Dargazany et al., 2014). In strain-induced crystallization, the crystal morphology maybe fringed-micelle, folded-chain, extended-chain, or a combination of these and further investigations are needed to elucidate the polymer-chain orientations. The type of orientations may have an influence on the mechanical properties of the formed material. In general, SIC results in anisotropy in the mechanical response and enhances the tensile stiffness and/or strength (Rao and Rajagopal, 2001). This enhancement in crystallinity of the material formed using SPIF indicates tremendous potential for using SPIF to form thermoplastic polymers.

Our future work will investigate methods to predict the maximum incremental depth that can be used without causing wrinkling or tearing of the sheet, with the goal of developing toolpath planning techniques for polymer SPIF that take this process mechanics into account. We will also perform experimental and computational work to investigate the damage evolution in polymer SPIF and evaluate the quantitative effects of shear and pressure on formability in the process. Additionally, we will investigate the crystal morphology and the thermo-mechanical properties of the material formed with SPIF to understand how the SPIF process parameters affect the properties of the formed material.

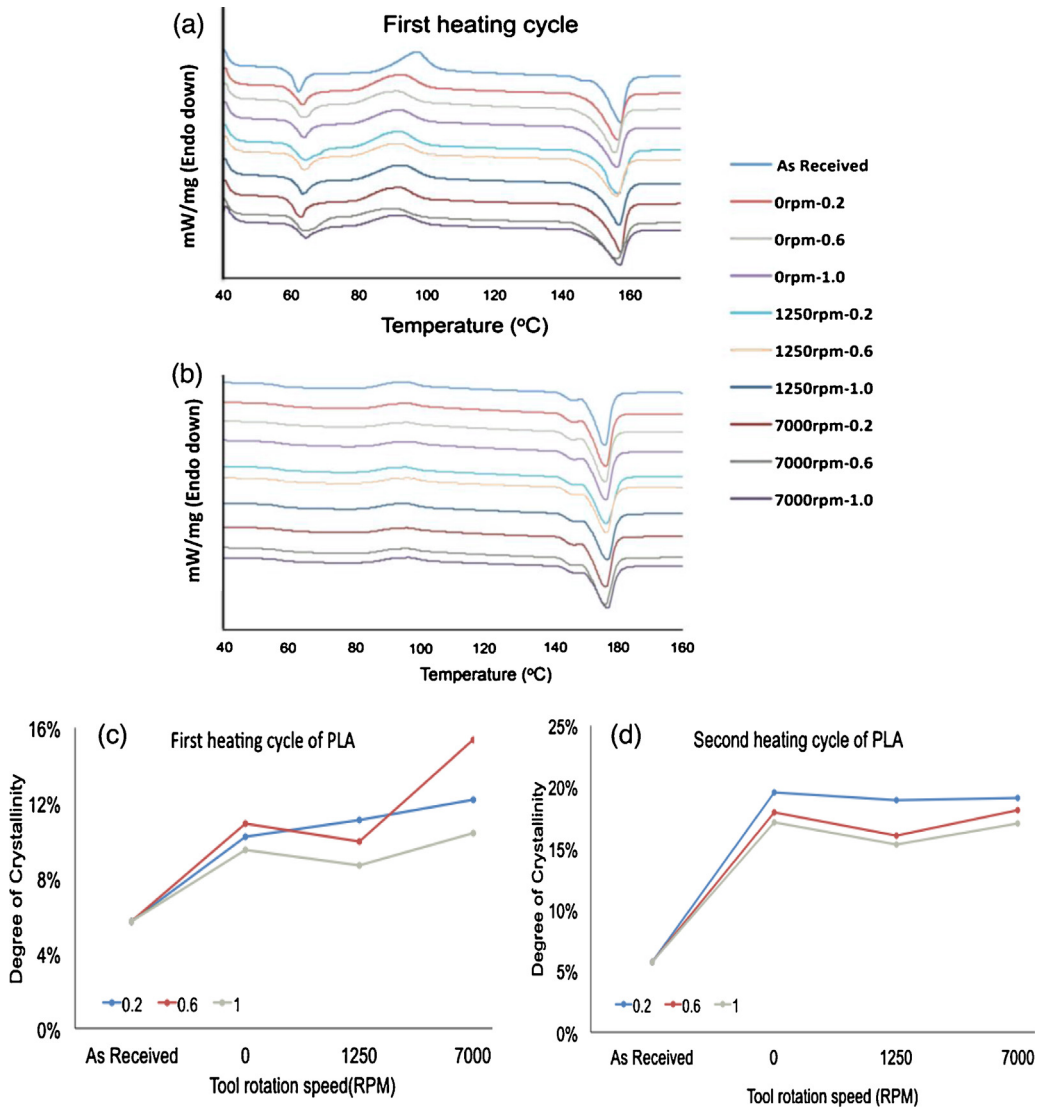

Fig. 14. Melting curves of PLA with different Δz and ω from the DSC measurements: (a) first heating cycle, (b) second heating cycle, (c) the crystallinity from the first heating cycle, and (d) the crystallinity from the second heating cycle.

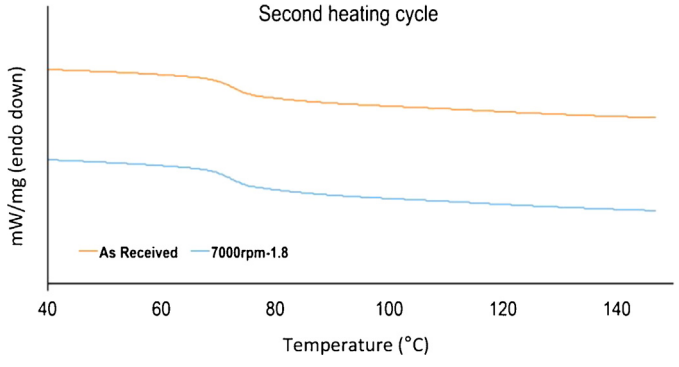

Fig. 15. Representative melting curves of PVC from the DSC measurements for the as-received material and of the material formed with SPIF at $\Delta z = 1.8$ mm and $\omega = 7000$ rpm.

References

Bouffioux, C., Eyckens, P., Henrard, C., Aerens, R., Van Bael, A., Sol, H., Duflou, J.R., Habraken, A.M., 2008. Identification of material parameters to predict single point incremental forming forces. Int. J. Mater. Form. 1 (1), 1147–1150.

Dargazany, R., Khiêm, V.N., Poshtan, E.A., Itskov, M., 2014. Constitutive modeling of strain-induced crystallization in filled rubbers. Phys. Rev. E 89, 022604–022616.

Duflou, J., Tunçkol, Y., Szekeres, A., Vanherck, P., 2007. Experimental study on force measurements for single point incremental forming. J. Mater. Process. Technol. 189 (1–3), 65–72.

Filice, L., Ambrogio, G., Micari, F., 2006. On-line control of single point incremental forming operations through punch force monitoring. CIRP Ann. – Manuf. Technol. 55 (1), 245–248.

Franzen, V., Kwiatkowski, L., Martins, P.A.F., Tekkaya, A.E., 2009. Single point incremental forming of PVC. J. Mater. Process. Technol. 209 (1), 462–469.

Franzen, V., Kwiatkowski, L., Neves, J., Martins, P.A.F., Tekkaya, A.E., 2008. On the capability of single point incremental forming for manufacturing PVC sheet parts. In: ICTP-2008, International Conference on Technology of Plasticity, Gyeongju, Korea.

Hodge, I.M., 1983a. Effects of annealing and prior history on enthalpy relaxation in glassy polymers. 4. Comparison of five polymers. Macromolecules 16 (6), 898–902.

Hodge, I.M., 1983b. Effects of annealing and prior history on enthalpy relaxation in glassy polymers. 3. Experimental and modeling studies of polystyrene. Macromolecules 16 (3), 371–375.

Hodge, I.M., Berens, A.R., 1982. Effects of annealing and prior history on enthalpy relaxation in glassy polymers. 2. Mathematical modeling. Macromolecules 15 (3), 762–770.

Hussain, G., Gao, L., 2007. "A novel method to test the thinning limits of sheet metals in negative incremental forming.". Int. J. Mach. Tools Manuf. 47 (3–4), 419–435.

Jackson, K., Allwood, J., 2009. The mechanics of incremental sheet forming. J. Mater. Process. Technol. 209 (3), 1158–1174.

Malhotra, R., Reddy, N.V., Cao, J., 2010. Automatic 3D spiral toolpath generation for single point incremental forming. J. Manuf. Sci. Eng. 132 (6), 061003.

Malhotra, R., Xue, L., Belytschko, T., Cao, J., 2012. Mechanics of fracture in single point incremental forming. J. Mater. Process. Technol. 212 (7), 1573–1590.
Martins, P.A.F., Bay, N., Skjoedt, M., Silva, M.B., 2008. Theory of single point incremental forming. CIRP Ann. – Manuf. Technol. 57 (1), 247–252.
Martins, P.A.F., Kwiatkowski, L., Franzen, V., Tekkaya, A.E., Kleiner, M., 2009. Single point incremental forming of polymers. CIRP Ann. – Manuf. Technol. 58 (1), 229–232.
Pilla, S., Gong, S., O'Neill, E., Rowell, R.M., Krzysik, A.M., 2008. Polylactide-pine wood flour composites. Polym. Eng. Sci. 48 (3), 578–587.
Pilla, S., Gong, S., O'Neill, E., Yang, L., Rowell, R.M., 2009. Polylactide-recycled wood fiber composites. J. Appl. Polym. Sci. 111 (1), 37–47.
Pratt, W.K., 1991. Digital Image Processing. John Wiley & Sons, New York.
Rao, I.J.R., Rajagopal, K.R., 2001. A study of strain-induced crystallization of polymers. Int. J. Solids Struct. 38 (6), 1149–1167.
Silva, M.B., Alves, L.M., Martins, P.A.F., 2010. Single point incremental forming of PVC: experimental findings and theoretical interpretation. Eur. J. Mech. A: Solids 29 (4), 557–566.
Turi, E.A. (Ed.), 1997. Thermal Characterization of Polymeric Materials, vol. 1, 2nd ed. Academic Press, p. 556.
Xu, D., Wu, W., Malhotra, R., Chen, J., Lu, B., Cao, J., 2013. Mechanism investigation for the influence of tool rotation and laser surface texturing (LST) on formability in single point incremental forming. Int. J. Mach. Tools Manuf. 73, 37–46.